Journal of Microelectronics and Electronic Packaging (2024) **21**, 42–49

ISSN: 1551-4897

Exploration of Interfacial Materials Chemistry Control to Improve Cu Wire-Bonding Reliability

Kevin Antony Jesu Durai, Dinesh Kumar Kumaravel, John Alptekin, Logan Estridge, Shyam Nair, and Oliver Chyan*

***Abstract*—Copper (Cu) wire bonding, with its advantages of higher electrical conductivity and better mechanical strength, has replaced gold wire bonding as a proven, cost-effective electrical interconnection solution for integrated circuit packaging for the past 15 y. Early Cu wire-bonding development required overcoming several technical challenges, including bond pad damage caused by copper's hardness and brittleness relative to gold. A more chemistry-related challenge of using Cu as a bonding wire is its well-known reactivity with oxygen. An inert atmospheric envelope of forming gas surrounding bonding capillary was developed to prevent the oxidation of Cu wire during electronic flame off to enable a strong bonding. Another more elusive materials-chemistry-related reliability challenge, with a typical low ppm occurrence, has been the chloride-induced corrosion defects between the Cu wire and Al bond pad. The opportunistic low-level chloride contaminations can originate from various points of the packaging manufacturing process flow, often rendering it untrackable. In this paper, we present recent efforts to systematically control interfacial materials chemistry across Cu-bonding wire, Cu-Al bimetallic contacts, and Cu_xAl_y intermetallic compounds to eliminate corrosion defects and improve the overall bonding reliability. The prevailing manufacturing solution is to utilize Pd-coated Cu-bonding wire that can only partially mitigate the Cu_xAl_y intermetallic corrosion vulnerability. We utilized a real-time corrosion screening metrology to explore the underlying interfacial materials chemistry that drives vigorous corrosion between Cu wire and Al bond pad when exposed to a trace level of chloride contaminant. Combined with scanning electron microscope, sensitive IR spectroscopy, and electrochemical characterization, our data show that strategic surface modification on both Cu-bonding wire and exposed Cu_xAl_y intermetallic can have a significant impact on reducing corrosion defect rates. The obtained mechanistic insights provide several new strategies enabled by a novel Cu-selective passivation coating technology to effectively mitigate Cu wire-bonding corrosion defects. Implications for improving overall Cu wire-bonding reliability will be presented based on these new approaches with low-cost and packaging-friendly advantages.**

***Keywords*—Cu wire-bonding failure, Cu-Al intermetallics, interfacial materials chemistry control, Cu-selective passivation coating technology**

The manuscript was received on November 29, 2023; revision received on March 18, 2024; accepted on April 11, 2024.

The original version of this paper was presented at the 56th International Symposium on Microelectronics (IMAPS'2023), San Diego, CA, USA, October 3-5, 2023.

Interfacial Electrochemistry and Materials Research Lab, University of North Texas, Denton, Texas 76201

*Corresponding author; email: oliverm.chyan@unt.edu

Introduction

Over the past decades, copper (Cu) has been used as a wire-bonding material because of its superior electrical conductivity, which is 40% higher than gold, and other attractive mechanical properties. The main reason, however, was the cost reduction compared with gold wire-bonding devices that were traditionally used. Several studies have explored the critical technical challenges that Cu wire bonding faces as the replacement for gold wire bonding in integrated circuit (IC) packaging [1, 2]. Harman and Johnson pointed out the complicated requirements and one of the potential technical obstacles involved in overcoming bond pad damage caused by Cu's hardness and brittleness compared with gold [2]. Jinzhi et al. reported that challenges like the reactivity of Cu toward oxygen have led to the development of forming gas (N_2:H_2) reductive atmosphere to prevent Cu oxidation while Cu wire bonding with Aluminum (Al) bond pad and also highlighted the advantages and challenges of Cu wire-bonding technology [3].

In addition, the problem of halide-induced corrosion of Cu wires and Al bond pads has been found to be one of the most significant reliability issues. Typically, these corrosion defects can also occur in the low ppm range from aggressive low-chloride impurities in the packaging process [4, 5]. One of the prevailing strategies to reduce these corrosion defects is the utilization of palladium (Pd)-coated Cu wire (PCC), which only partially solves the corrosion problem [6-8]. Singh et al. reported earlier that various reliability tests done on PCC wire-bonded devices showed great intermetallic compound (IMC) coverage with a flat bonding interface but still resulted in reliability failure because of anomalous chloride levels [6]. Xu et al. studied the behavior of PCC wire and its impact on IMC growth in those wire-bonding devices and reported the IMC corrosion problem [9]. Meanwhile, Lee et al. reported mechanical reliability studies comparing PCC and Cu wire, where both showed the same chloride-induced corrosion resistance if Cu-Al IMC formation was properly formed [10]. Although Lim et al. and Wu et al. studied the corrosion performance of Cu-Al IMC with the effect of Pd addition, showing slightly improved corrosion resistance in Cu and Cu-Al samples [11, 12]. However, controlling the distribution of Pd at the ball bond interface poses a challenge, leaving this metallurgical solution to inhibit the growth of IMCs subject to potential imperfections due to the unpredictability of the ball melting process.

To better understand the mechanism of interfacial corrosion, numerous researchers have reported the behavior of Cu-Al IMC under different test conditions [13-16]. In particular, Kim et al. have explored the effect/importance of Cu-Al IMC formation on Cu wire and Al bond pad using mechanical test systems to study the failure mode of ball fractures and also reported the Cu_9Al_4 IMC as the predominant IMC at wirebonding temperatures (150-300°C) [14]. Meanwhile, Boettcher et al.'s further investigated the corrosion rate of the Cu-Al IMC species at the interface, finding that the Cu-rich phase corrodes faster compared with the Al-rich phase [17]. Liu et al. also studied the corrosion behavior of Cu-Al IMC in a chloride environment, resulting in selective IMC corrosion with a high corrosion rate [4].

Further research has focused on evaluating the effects of epoxy molding compounds (EMCs) with two key factors, pH levels and Cl^- content, toward the substrate material properties on the reliability of Cu wire ball grid array compounds [18] and developing new Cu wire materials coated with highly reliable and corrosion-resistant gold-palladium [19]. These studies offer valuable insights and potential directions for future research in ongoing efforts to enhance the dependability and effectiveness of Cu wire bonding in microelectronics. Nonetheless, managing the interfacial materials chemistry to minimize corrosion-related defects and enhance bonding reliability remains a complex challenge that the industry still faces.

In our prior research, we found that a Cu-Al bimetallic contact significantly accelerates galvanic corrosion. Using a micropattern test platform, we observed accelerated Al corrosion, even without IMCs present. Real-time corrosion screening showed corrosion progression on both the Cu-bonding ball and Cu microdots on Al [20, 21]. We identified hydrogen gas evolution as a critical factor for Cu ball bond liftoff and wire-bonded device failure. We also examined the role of IMCs corrosion in wirebond liftoff failure, a primary cause of device failure (Fig. 1). We demonstrated the effectiveness of a specific Cu-selective passivation coating and a corrosion inhibitor, "inhibitor A" in preventing hydrogen evolution reactions and bimetallic corrosion in the Cu-Al system. Our tests of coated devices showed complete protection against Cu ball liftoff under extreme corrosion conditions [21]. These findings solve a significant reliability issue in wirebonding devices and guide future research on corrosion mechanisms and mitigation strategies.

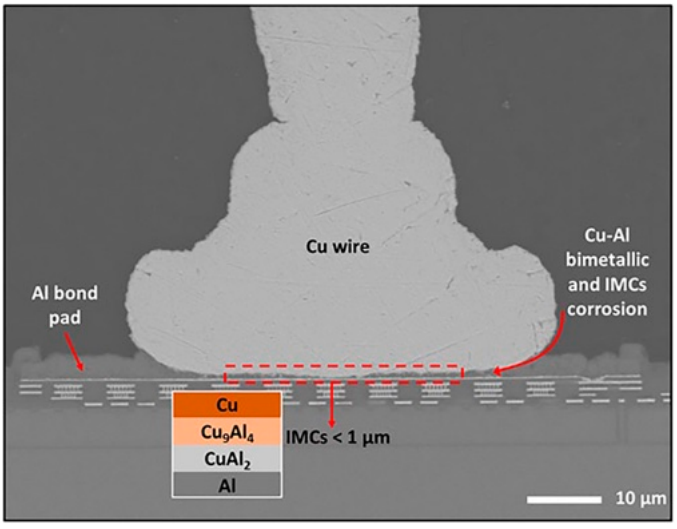

Fig. 1. Cross-section image of Cu-Al ball bond interface.

In this paper, we address the chloride-based corrosion issue by discussing the development of a copper-selective passivation coating that offered over 90% protection according to our in-situ accelerated tests. We have also utilized our developed mechanistic understanding of the Cu-Al galvanic corrosion [21] and applied this understanding to investigate the corrosion behavior of the Cu-Al wire bond under an extremely corrosive environment of 600 ppm Cl^- aqueous solution. First, we performed a zero resistance ammetry (ZRA) electrochemical study on the various galvanic couples possible in the Cu-Al wire bond when submerged in 600 ppm Cl^- over time to determine their current densities—both with and without the addition of inhibitor A to the solution. In addition, we constructed a Tafel plot of each species in the Cu-Al wire bond under 600 ppm Cl^- environment via potentiodynamic polarization to investigate the individual corrosion rate of each metal and IMC—with and without inhibitor A.

In addition to electrochemical experiments, Fourier transform infrared spectroscopy (FTIR) was employed to assess the chemical bonding characteristics of metals and intermetallic compounds (IMCs). This technique facilitates the identification of chemical adsorption of the inhibitor (chemisorption), and also tracks the formation of copper oxide during corrosion processes. To determine the effect of our passivation coating on actual wire-bonded devices, we employed our real-time corrosion screening metrology, where wire-bonded devices (unencapsulated) were submerged in 600 ppm Cl^- solution for a total of 2 h and analyzed by an optical microscope for a wire bond liftoff failure. Effective prevention of the corrosion mechanism requires a uniform and defect-free passivation coating application on the Cu wire, providing a physical barrier to hydrogen evolution. To test the uniformity of the developed inhibitor coating, we employed a microetching procedure on blanket Cu surfaces—both with and without passivation coating and investigated the surface modification via optical microscopy. Finally, we verified the adhesive strength between the passivation coating and the epoxy molding compound by tensile pull testing, as performed on blanket Cu surfaces—with and without passivation coating. FTIR spectroscopy was used to determine the breaking point in the Cu-inhibitor-epoxy interface.

Experimental

A. Electrode Preparation

The Cu-Al IMC electrode preparation method was already reported in our previous work on studying Cu IMC corrosion with a passivation strategy [22]. In our past work, pure Cu and Al alloyed with 0.5% Cu blanket wafers (~2 µm) were used [22]. However, in this work, the Cu-Al IMC was prepared as follows: Si wafers were sputtered with a thin layer of Ti (for adhesion) and Ru (as a barrier layer between Cu-Al IMCs and Si). Then, using the Denton Vacuum Desktop pro sputtering unit, ~400 nm of Cu-Al IMCs were deposited by cosputtering of Cu and Al. After sputtering, IMCs were annealed at 400°C in a nitrogen environment for 1 h in a Lindberg/Blue Mini-Mite Tube Furnace. Different compositions of Cu-Al IMCs

were confirmed by a Rigaku SmartLab X-ray Diffractometer by grazing angle XRD at a 0.5° incident angle relative to the surface plane.

B. Potentiodynamic Polarization and Zero Resistance Ammetry

All electrochemical experiments in this work were performed on a CH Instruments 760D Potentiostat. As discussed in our previous work [22], potentiodynamic polarization (Tafel Plot) was done by a three-electrode system utilizing a Pt counter electrode and Ag/AgCl in a saturated KCl reference electrode with a scan rate of 1 mV/s. The potential window was set after 10 min of stable open circuit potential when samples were immersed in the electrolyte solution. ZRA was used to measure the direct galvanic current of different metals and IMCs in the bonding interface. In this setup, the more noble metal/IMC will act as the cathode, and the least noble metal/IMC will act as the anode. This ZRA measurement was carried out for 12 h in various corrosive solutions. The current measured from this experiment will be converted to current density, calculated by dividing the obtained current by the surface area (~0.57 cm^2). ACS grade NaCl was used to prepare 600 ppm Cl^- solution with 18.2 MΩ·cm ultrapure water from a Millipore Sigma water purification system.

C. ATR-IR of PostElectrochemistry Electrodes

After electrochemistry, IMC electrodes were gently rinsed with ultrapure water and allowed to air dry in a clean room environment before taking ATR-IR (attenuated total reflectance-IR) spectra. A Bruker Invenio FTIR spectrometer equipped with a deuterated triglycine sulfate detector and a Diamond ATR accessory was utilized for measurements. Background measurements were carried out on a set of as-prepared IMCs, Al and Cu before the respective postelectrochemistry electrodes were measured. An integration of 300 scans was utilized for each background and sample measurement. Standard automatic atmospheric corrections, built into Bruker's OPUS software, were carried out to remove water vapor and carbon dioxide peaks, resulting from imperfect background cancellations.

D. Corrosion Immersion Screening with and Without Passivation Coating

For live microscopic corrosion screening and optical images, a Nikon LV150N metallurgical microscope with a digital camera was used, as explained in our previous work [20]. For corrosion screening, 600 ppm Cl^- solution was used, as also utilized in the electrochemical experiment. Test devices with Cu-Al wire bonds (unencapsulated) from commercial sources were used for the entire corrosion screening studies, from that some of the devices will be coated by our Cu-selective passivation coating [23]. Scanning electron microscope (SEM) imaging was conducted in a JEOL IT200 at 15 kV under a high vacuum using a secondary electron detector.

E. Microetching Analysis to Determine Coating Uniformity on Cu Surface

To obtain proper corrosion protection on those Cu-Al wirebonding devices, the passivation coating should be uniform and defect-free. A micro wet-etching technique developed in our laboratory was used to provide information on localized coating defects and inhomogeneities. The chemistry of the chosen wet etchant is based on common printed circuit board etching protocols in the semiconductor industry. The etchant used is an acidic cupric chloride and hydrochloric acid solution. It works by oxidizing the Cu(0) surface (and in turn, reducing the Cu(II) species in etch solution).

$$CuCl_2 + Cu \rightarrow 2CuCl \quad (1)$$

The role of hydrochloric acid is to dissolve and solubilize the cuprous chloride formed on the surface so that the cupric chloride etchant can continue oxidizing the underlying Cu(0) [24]. For this work, a dilute concentration of 20 mM $CuCl_2$ solution was used as the Cu microetchant. Test Cu wafers with coatings were immersed for 1 min in the microetchant solution and thoroughly rinsed with ultra-pure water immediately after removal.

F. EMC Adhesion Strength Testing

EME-G700 Type LG and EME-G631HA Type C EMCs from Sumitomo Bakelite Ltd. were used for adhesion testing. Semiconductor-grade copper lead frame substrates (Cu-LFs) were used to mimic the copper ball bond surface. Tensile pull-testing, evaluating the strength of the EMC adhesion, was conducted in the UNT Center for Friction Stir Processing with the custom-made mini tensile tester [25]. The Button shear test was conducted at the Sumitomo facility, and ATR-IR spectra were obtained using a Bruker Invenio FTIR spectrometer. For adhesion testing, 8 × 8 mm square cutouts of Cu-LFs were taken and coated with an inhibitor using our solvent-based process. Epoxy molding of Cu-LFs was carried out at 175°C under a heated pressure block and cured for another 2 h at 175°C [26]. Then, those epoxy-molded (coated and noncoated) Cu-LFs went for pull testing.

Results and Discussion

A. Galvanic Corrosion Behavior in 600 ppm Cl^- and Influence of 0.1% wt/v Inhibitor

Galvanic corrosion current behavior for possible couples in the Cu-Al wire bond interface (Cu:Al, Cu:Cu_9Al_4, Cu_9Al_4:$CuAl_2$, and $CuAl_2$:Al) was studied using 600 ppm Cl^- solution with and without 0.1% wt/v inhibitor. The average current densities over 12 h of immersion time are shown in Fig. 2. The trend of the current densities for the control couples (without inhibitor) observed was as follows: Cu:Al > $CuAl_2$:Al > Cu_9Al_4:$CuAl_2$ > Cu:Cu_9Al_4. There is one key difference from our previous study in 100 ppm Cl^- solution [22], namely the Cu:Cu_9Al_4 couple now has only slightly less current density than the Cu_9Al_4:$CuAl_2$ couple, instead of dramatically less. As the concentration of Cl^- in solution is greater in this study, the equilibrium of the anodic reaction is shifted toward the right, i.e., toward more oxidation and a higher corrosion rate.

To explain the relative trends of current densities in Fig. 2, the current density is the highest in the Cu:Al couple, as these two metals have the highest difference in standard reduction potentials (~2 V) of any two species present. The next highest is the $CuAl_2$:Al couple, which is higher than the other two IMCs due to its more Al-rich nature. As explained in our

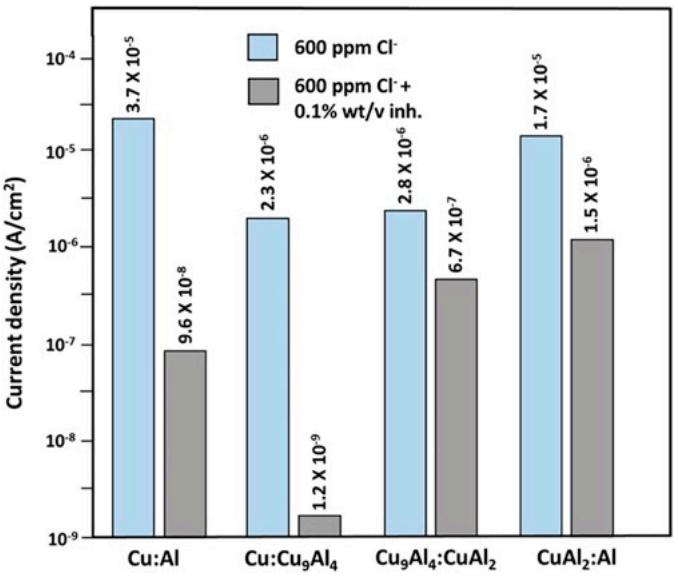

Fig. 2. Average current density values obtained from ZRA for 12 h in 600 ppm Cl^- with and without inhibitor.

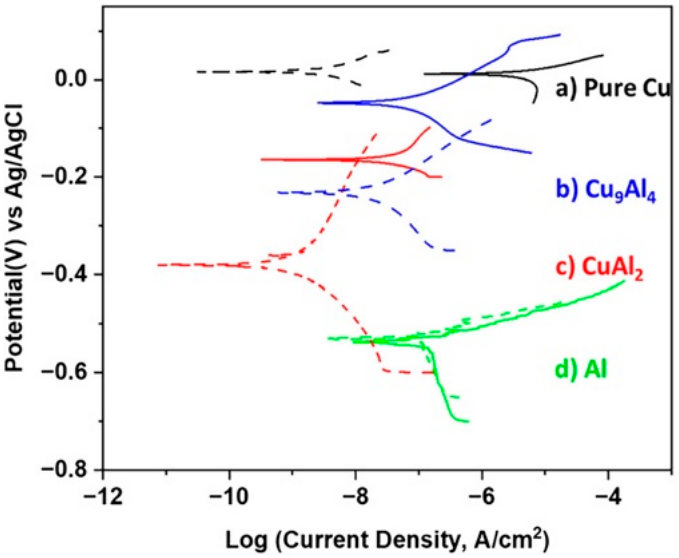

Fig. 3. Tafel plots of the metals and alloys utilized in this study in 600 ppm Cl^- (solid lines) and 600 ppm Cl^- + 0.1% inhibitor (dotted lines) for (a) pure Cu, (b) Cu_9Al_4, (c) $CuAl_2$, and (d) Al.

previous work [23], this higher current density in $CuAl_2$:Al is likely due to a dealloying process of $CuAl_2$ caused by localized pitting corrosion and selective microcorrosion of the less noble Al within the $CuAl_2$, facilitated by chloride breaking down the protective Al oxides [27, 28].

As for the condition including 0.1% wt/v of inhibitor (Fig. 2), the trend of the current densities was $CuAl_2$:Al > Cu_9Al_4:$CuAl_2$ > Cu:Al ≫ Cu:Cu_9Al_4. This trend was also different from our prior study with 100 ppm Cl^- solution [23], which was as follows: Cu:Al > $CuAl_2$:Al ≫ Cu_9Al_4:$CuAl_2$ > Cu:Cu_9Al_4. When comparing the differences between 100 and 600 ppm Cl^- it was revealed that the magnitudes of the current densities of Cu:Al and Cu_9Al_4:$CuAl_2$ are nearly identical, whereas the current densities of Cu_9Al_4:$CuAl_2$ and $CuAl_2$:Al increased dramatically from 100 to 600 ppm Cl^-. This further supports the hypothesis of the dealloying of $CuAl_2$ species, as facilitated by an extremely harsh Cl^- environment [28, 29].

Overall, the addition of 0.1% wt/v of inhibitor into 600 ppm Cl^- solution resulted in a reduction in current density for all the metal/IMCs, which shows the effectiveness of our inhibitor not only toward the Cu-Al galvanic system but also with the different contact variation of metal/IMC's galvanic corrosion. Most importantly, the study suggested the corrosion protection potential of developing a new passivation coating based on this inhibitor, shown in a later section, even in an extremely harsh 600 ppm chloride environment.

B. Individual Corrosion Behaviors in 600 ppm Cl^- and Influence of 0.1% wt/v Inhibitor

Fig. 3 shows collective Tafel plots for individual metals in 600 ppm Cl^- solution with and without inhibitor. It is very evident that the addition of 0.1% wt/v of the inhibitor has a huge impact on the decreased corrosion current density and individual corrosion rate for each metal and IMC. When the inhibitor was added, the corrosion potential (E_{corr}) of Cu shifted to a slightly more positive value, whereas for Al and Al-containing alloys E_{corr} shifted to more negative values. As mentioned in our previous work [22], inhibitor A suppresses bimetallic corrosion in the Cu:Al system by inhibiting the cathodic hydrogen evolution reaction on the Cu surface. This change in E_{corr} might be because our passivation coating is only Cu selective, this leads the Al component in Cu-Al IMCs to undergo Al_xO_y formation to dominate the overall electrochemical behavior and move the E_{corr} to a more negative side.

C. Interfacial Characterization of Electrodes After ZRA by ATR-IR Spectroscopy

After ZRA in chloride solution, ATR-IR of the electrodes (Fig. 4) demonstrated the growth of Cu(I) oxide, based on 650 cm^{-1} IR absorption peaks, on Cu and Cu-Al IMCs only and a relatively flat spectrum for Al. This is the expected result since the corrosion solution does not contain any organic species able to bind strongly to the surface of the electrodes. Without any corrosion inhibitor in solution, the surfaces of the electrodes readily corrode and oxidize, as both Cu and Al are well-known to undergo pitting corrosion in the presence of chloride [30, 31]. The evolution of Cu(I) oxide (650 cm^{-1}) could have originated from the solution-assisted oxidation of Cu due to dissolved

Table I
Tafel Plot Calculations of the Metals and IMCs in 600 ppm Cl^- Solution with and without 0.1% Inhibitor

Sample	E_{corr} (V)	I_{corr} (A/cm^2)
Cu in 600 ppm Cl^-	0.013	9.1×10^{-7}
Cu in 600 ppm Cl^- + 0.1% inh.	0.023	1.7×10^{-8}
Cu_9Al_4 in 600 ppm Cl^-	−0.06	1.3×10^{-8}
Cu_9Al_4 in 600 ppm Cl^- + 0.1% inh.	−0.23	3.5×10^{-9}
$CuAl_2$ in 600 ppm Cl^-	−0.16	1.1×10^{-7}
$CuAl_2$ in 600 ppm Cl^- + 0.1% inh.	−0.39	3.8×10^{-8}
Al in 600 ppm Cl^-	−0.51	4.8×10^{-6}
Al in 600 ppm Cl^- + 0.1% inh.	−0.53	3.4×10^{-7}

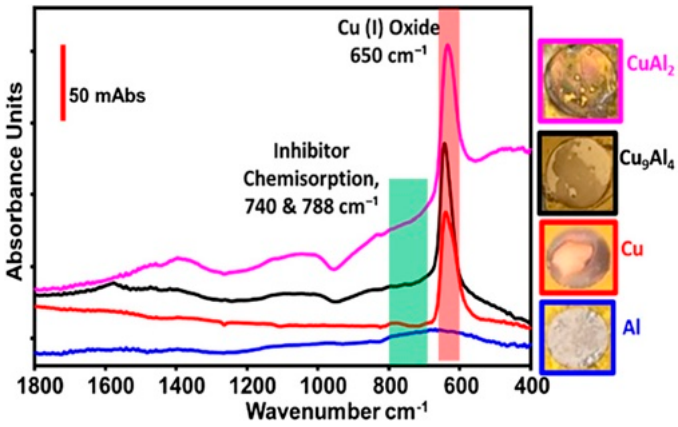

Fig. 4. ATR-IR spectra of the metals and alloys after ZRA in Cl^- solution. From top to bottom: $CuAl_2$, Cu_9Al_4, Cu, Al.

oxygen and adsorption of -OH on Cu in water [30]. Additionally, CuCl surface products are hypothesized to react with water to form Cu(I) oxides at low chloride concentrations [31].

After ZRA measurement in 600 ppm chloride with the addition of 0.1% inhibitor, ATR-IR collected on the electrodes (Fig. 5) demonstrated almost no Cu oxidation, making the electrodes appear less corroded. Furthermore, it was shown that the inhibitor prevented corrosion on the Cu and Cu-Al IMCs, and verified to chemisorb onto the IMC surfaces via the presence of the peaks located at 740 and 788 cm^{-1} wavenumbers, even despite thorough rinsing of electrodes before ATR-IR measurement. The inhibitor also suppressed the formation of Cu(I) oxides compared with the electrodes submerged in only chloride. Thus, the inhibitor prevents both the anodic dissolution of the electrodes and their Cu oxide formation. Another important observation, the bottom ATR-IR spectrum of the Al electrode surface showed no sign of an adsorbed inhibitor. The absence of an adsorbed inhibitor on the Al metal surface suggests the inhibitor adsorption is Cu-selective.

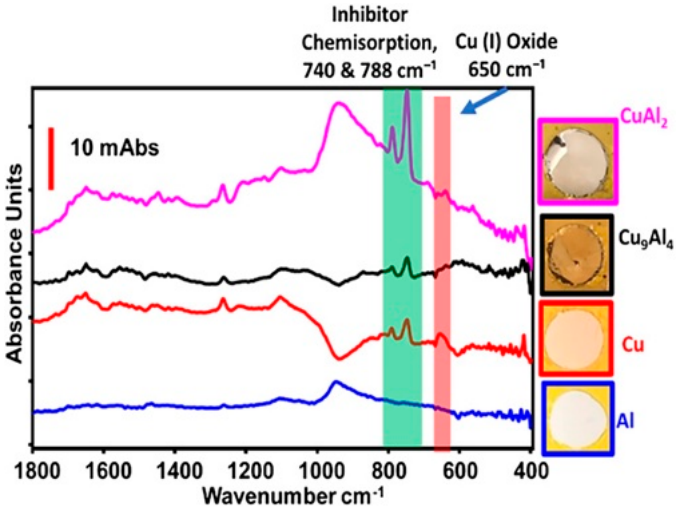

Fig. 5. ATR-IR spectra of the metals and alloys after ZRA in Cl^- + 0.1% inhibitor. From top to bottom: $CuAl_2$, Cu_9Al_4, Cu, Al.

D. *Corrosion Immersion Screening on Cu-Al Wire-Bonded Devices*

To evaluate the corrosion protection achieved by our passivation coating, two distinct samples were compared: the as-received (non-coated) Cu-Al device and the device with passivation coating. The corrosion immersion screening was conducted by placing the two distinct sample devices in a severely corrosive environment of 600 ppm Cl^- aqueous solution, which is much more corrosive than the typical operating condition employed in thermal stress testing by the IC packaging sector. After 2 h of corrosion screening, non-coated devices showed over 93% of severe Cu wire-bonding liftoff (Fig. 6a). As discovered in our previous work [21], galvanic corrosion was initiated between the Cu-Al-bonding interface with Al_xO_x dendrite formation and H_2 gas evolution. Fig. 6b demonstrates a Cu wire liftoff after Al bond pad corrosion. Subsequently, the corrosion expands toward the Cu-Al IMCs and causes a weak Cu-Al bond interface, culminating in Cu wire liftoff and shifting away from the Al bond pad. On the other hand, Cu-Al devices with passivation coating encountered less than 15% of wire liftoff (Fig. 7a) after 2 h exposure to a highly corrosive 600 ppm Cl^- aqueous solution. In our previous work [22], we successfully achieved 0% wire bond liftoff after 2 h submersion in 100 ppm Cl^- solution. SEM images from Fig. 7b display a coated device without any corrosion on the Al bond pad and no detachment of the copper wire. By preventing the crucial process of cathodic H_2 evolution through the application of our passivation coating, the galvanic-induced corrosion caused between the Cu-Al-bonding interface was significantly retarded [21].

E. *Evaluation of Coating Uniformity on Cu Surface Using Microetching Analysis*

Using the microetching screening method, it is possible to detect whether there are any defects or nonuniformities present on the coated Cu substrate. This analysis primarily functions through the oxidation of copper (Cu(0)) on the substrate's

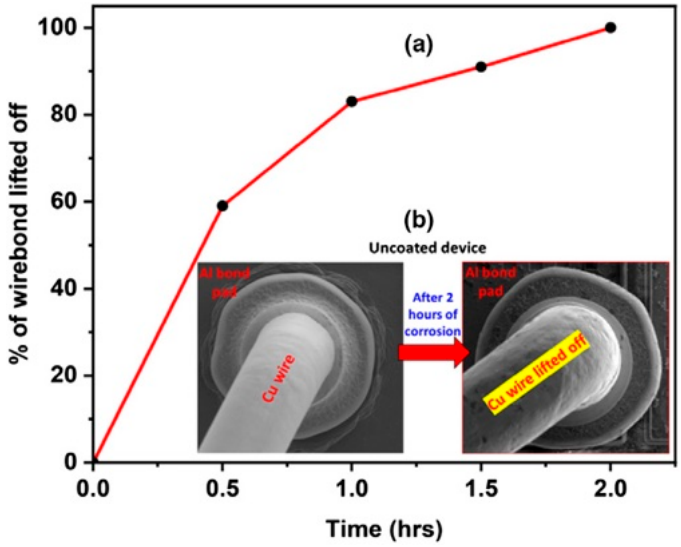

Fig. 6. Corrosion immersion screening of uncoated Cu-Al wire-bonded device in 600 ppm Cl^-. (a) The plot shows % of wire-bonds lifted off after 2 h immersion in a corrosive medium and (b) SEM image of the initial and after 2 h of corrosion study.

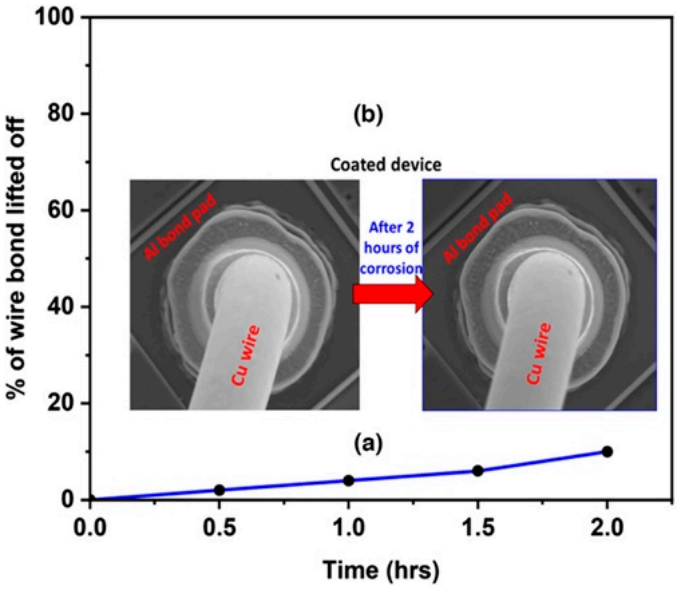

Fig. 7. Corrosion immersion screening of coated Cu-Al wire-bonded device in 600 ppm Cl^-. (a) The plot shows % of wire-bonds lifted off after 2 h immersion in a corrosive medium and (b) SEM image of the initial and after 2 h immersion.

surface, leading to the formation of cuprous chloride (CuCl) (eq. (1)). This selective chemical etching is vigorous on copper especially when no protective coating is present. In the context of the optical imaging and SEM results, the distinct outcomes between the bare Cu substrate and the passivation-coated Cu substrate can be attributed to the uniformity and defect-free nature of the passivation layer. For the bare Cu substrate, the etching process unveils the polycrystalline structure of Cu, which becomes evident in optical images after just 1 min of etching. Further SEM analysis of the surface also confirms the formation of Cu-polycrystalline grains and CuCl, as shown in Fig. 8a. Conversely, the passivation-coated Cu substrate shows no significant changes when subjected to the same etching conditions, as observed in the optical and SEM images (Fig. 8b). This lack of reaction underscores the effectiveness of the passivation layer in shielding the copper surface from the etchant. The uniform and defect-free nature of the passivation coating ensures that the underlying copper remains unaffected by the etchant, thus confirming the coating's stability.

F. EMC Adhesion Strength Testing with Passivation Coating

To avoid any delamination-associated reliability issues between EMC and the passivation coating, adhesion compatibility was tested with the tensile pull test and the button shear test. Table II presents a comparative analysis of the tensile pull strength between uncoated and passivated copper lead-frames (Cu-LFs) when exposed to EMC. The tensile pull test showed that bare Cu-LFs possessed a pull strength of 30 N, indicating strong adhesion properties. On the other hand, the passivation-coated Cu-LFs demonstrated a significantly lower pull strength of 16 N. This pattern of reduced strength in the presence of a passivation layer was also observed in the button shear test, with bare Cu-LFs registering a strength of 134.6 N, in contrast to 61.1 N for coated Cu-LFs.

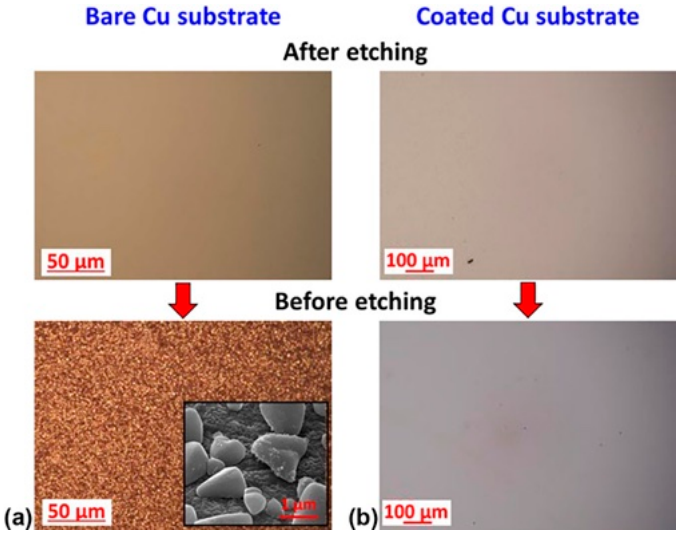

Fig. 8. Optical image before and after microetching (a) Bare Cu (inset—SEM image of Cu-polycrystalline grains) (b) coated Cu.

Table II
Adhesion Pull Strength with EMC on Bare Cu-LFs and Passivation Layer Coated Cu-LFs

Test no.	Test method	Surface finishing	Pull strength (N)
1	Tensile pull test	Bare Cu (controlled)	30
2		Passivated Cu	16
3	Button shear test	Bare Cu (controlled)	134.6
4		Passivated Cu	61.1

Complementing these mechanical tests, ATR-IR spectroscopy analysis provided insight into the chemical interactions at the breakage points during the postpull test. Fig. 9 illustrates the ATR-IR spectra with distinct absorption bands associated with the materials involved. Aromatic C-H stretching and $Si-CH_3$ within the 700-800 cm^{-1} region and a significant broad absorbance between 900 and 1,150 cm^{-1}. This latter region reveals peaks at 1,020 cm^{-1} and a shoulder at 1,100 cm^{-1},

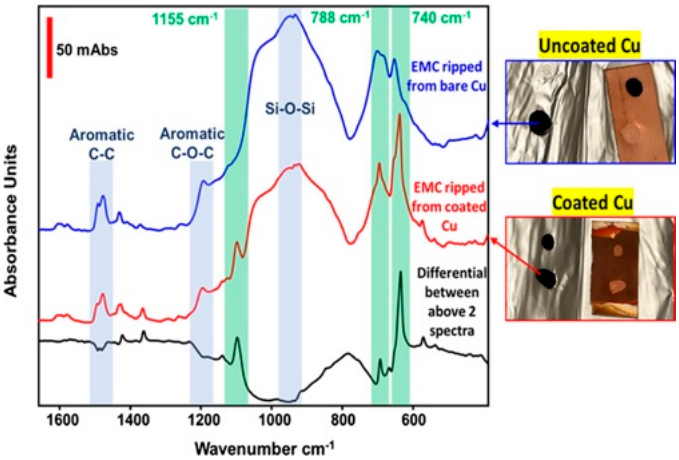

Fig. 9. ATR-IR spectra showing coating leftover on the EMC ripped from the sample surface.

corresponding to Si-O-Si and Si-O-C bonding, respectively, consistent with known silica fillers in EMC. The differential spectra between the coated and noncoated samples showed the presence of passivation coating on the epoxy, which was confirmed by the 788 and 740 cm^{-1} peaks. Notably, these findings indicate that the failure point during the pull test occurs within the coating layer itself rather than at the interface between the EMC and the coating layer. This evidence further substantiates the bonding efficacy of the passivation coating with EMC, despite the observed reduction in mechanical adhesion strength.

Conclusions

In this work, the challenges and solutions for improving Cu wire-bonding reliability against chloride-induced corrosion defects were studied through interfacial materials chemistry control.

1. The galvanic corrosion behavior of various couples of Cu-Al and IMCs was investigated in a highly corrosive 600 ppm Cl^- environment. In general, adding a mere 0.1% inhibitor to the solution reduced the average current density values obtained from the ZRA technique after 12 h of immersion time by several orders of magnitude over the control. Potentiodynamic polarization also supports the ZRA results where the I_{corr} reduces with the addition of the inhibitor.
2. Post FTIR analysis on Cu-Al IMC samples that underwent ZRA in 600 ppm Cl^- solution with added inhibitor shows a lack of Cu(I) oxide and exhibits the chemisorption of inhibitor on Cu-Al IMCs.
3. Corrosion immersion screening in 600 ppm Cl^- solution supported our previous work results where only 15% of Cu wire liftoff was recorded.
4. Micro-etching analysis on inhibitor-coating blanket Cu surface confirmed the coating's uniformity and defect-free nature.
5. We have also verified the adhesive strength between the inhibitor and the EMC through various pull testing and used FTIR spectroscopy to determine that the breaking point in the Cu-inhibitor-EMC interface is not between EMC-inhibitor; however, the inhibitor's chemical-bonding signature was found on both the EMC and Cu surface.

Acknowledgments

The authors would like to thank NXP Semiconductors for financially supporting this work, Sumitomo for helping us with Button shear test results, Dr. Rajiv Mishra from UNT Materials Science & Engineering and Center for Friction Stir Processing for helping us with tensile pull testing, and the University of North Texas Materials Research facility for their instrumentation support.

References

[1] C.D. Breach, "What is the future of bonding wire? Will copper entirely replace gold?" *Gold Bulletin*, Vol. 43, pp. 150-168, 2010.

[2] G.G. Harman and C.E. Johnson, "Wire bonding to advanced copper, low-K integrated circuits, the metal/dielectric stacks, and materials considerations," *IEEE Transactions on Components and Packaging Technologies*, Vol. 25, pp. 677-683, 2002.

[3] L.L. Jinzhi, C. Yan, W. Bisheng, L. Xiaomin, F. Chao, and H. Younan, "A review on the copper bond pad application in wire bond technique," *IEEE*, pp. 1546-1553, 2018.

[4] D. Liu, H. Chen, J. Wu, and E. Then, "Corrosion behavior of Cu-Al intermetallic compounds in copper wire bonding in chloride-containing accelerated humidity testing," IEEE, pp. 629-636, 1 May, 2016.

[5] V. Mathew, E. Wikramanayake, and S.F. Chopin, "Corrosion of copper wire bonded packages by chlorine containing foreign particles," IEEE, pp. 504-511, Jun 2020.

[6] I. Singh, S. Low, S.F. Song, C.S. Jung, L.M. San, I. Qin, C. Huynh, H. Clauberg, S.T. Nguyen, B. Chylak, H. Xu, and V.L. Acoff, "Pd-coated Cu wire bonding reliability requirement for device design, process optimization and testing," International Symposium on Microelectronics 2012, San Diego, California, pp. 396-404, 2012.

[7] W. Koh, T. Lee, H. Ng, K. Goh, H. Ho, "Investigation of palladium coverage on bonded balls of palladium-coated copper wires," 12th International Conference on Electronic Packaging Technology and High-Density Packaging. 1-7, 10.1109/ICEPT.2011.6066818 Shanghai, China, pp. 56-60, 2011.

[8] S. Nemoto, T. Maeda, M. Miyajima, Y. Akaike, K. Kitagawa, H. Ishii, H. Shimamoto, and K. Kikuchi, "Investigation of mechanism of corrosion resistance of Pd coated Cu wire joint by pseudo process," Japan Institute of Electronics Packaging, pp. 56-60, Apr 2019.

[9] H. Xu, I. Qin, H. Clauberg, B. Chylak, and V.L. Acoff, "Behavior of palladium and its impact on intermetallic growth in palladium-coated Cu wire bonding," *Acta Materialia*, Vol. 61, pp. 79-88, 2013.

[10] C.S. Lee, T. Tran, D. Boyne, L. Higgins, and A. Mawer, "Copper versus palladium coated copper wire process and reliability differences," IEEE, pp. 1539-1548, May 2014.

[11] A.B.Y. Lim, W.J. Neo, O. Yauw, B. Chylak, C.L. Gan, and Z. Chen, "Evaluation of the corrosion performance of Cu–Al intermetallic compounds and the effect of Pd addition," *Microelectronics Reliability* , Vol. 56, pp. 155-161, 2016.

[12] Y. Wu, S.C. Barton, and A. Lee, "Galvanic corrosion behavior at the Cu-Al ball bond interface: Influence of Pd addition and chloride concentration," *Microelectronics Reliability* , Vol. 92, pp. 79-86, 2019.

[13] H. Xu, I. Qin, H. Clauberg, B. Chylak, and V.L. Acoff, "New observation of nanoscale interfacial evolution in micro Cu–Al wire bonds by in-situ high resolution TEM study," *Scripta Materialia*, Vol. 115, pp. 1-5, 2016.

[14] H.-J. Kim, J.Y. Lee, K.-W. Paik, K.-W. Koh, J. Won, S. Choe, J. Lee, J.-T. Moon, and Y.-J. Park, "Effects of Cu/Al intermetallic compound (IMC) on copper wire and aluminum pad bondability," *IEEE Transactions on Components and Packaging Technologies*, Vol. 26, pp. 367-374, 2003.

[15] Y.H. Lu, Y.W. Wang, B.K. Appelt, Y.S. Lai, and C.R. Kao, "Growth of CuAl intermetallic compounds in Cu and Cu(Pd) wire bonding," 2011 IEEE 61st Electronic Components and Technology Conference (ECTC), 2011.

[16] C.L. Cha, H.J. Chong, H.G. Yaw, M.Y. Chong, and C.H. Teo, "Cu-Al intermetallic growth behaviour study under high temperature thermal aging," IEEE, pp. 1-5, Sep 2018.

[17] T. Boettcher, M. Rother, S. Liedtke, M. Ullrich, M. Bollmann, A. Pinkernelle, D. Gruber, H. Funke, M. Kaiser, K. Lee, M. Li, K. Leung, T. Li, M.L. Farrugia, O. Halloran, M. Petzold, B. März, and R. Klengel, "On the intermetallic corrosion of Cu-Al wire bonds," IEEE, pp. 585-590, Dec 2010.

[18] P. Su, H. Seki, Y. Nishitani, C. Ping, S. Zenbutsu, S. Itoh, L. Huang, N. Liao, B. Liu, C. Chen, W. Tai, and A. Tseng, "An evaluation of effects of molding compound and substrate material properties on reliability of Cu wire BGA components," IEEE 62nd Electronic Components and Technology Conference, San Diego, CA, USA, pp. 1110-1116, [10.1109/ECTC.2012.6248974], 2012.

[19] S. Klengel, R. Klengel, J. Schischka, T. Stephan, M. Petzold, M. Eto, N. Araki, and T. Yamada, "A new reliable, corrosion resistant gold-palladium coated copper wire material," IEEE, pp. 175-182, May 2019.

[20] M. Asokan, J. Caperton, Z. Thompson, O. Chyan, M. Chowdhury, S. O'Connor, and L. Nguyen, "Novel corrosion prevention treatments for Cu wire bonded device to improve bonding reliability," IEEE, pp. 139-143, May 2018.

[21] N. Ross, M. Asokan, G.I. Ashok Kumar, J. Caperton, J. Alptekin, A.S. Salunke, and O.M. Chyan, "Mechanistic study of copper wire-bonding failures on packaging devices in acidic chloride environments," *Microelectronics Reliability* , Vol. 113, pp. 113917, 2020.

[22] J. Alptekin, E. Gopalakrishnan, D.K. Kumaravel, K. Antony, H. Langerak, O. Chyan, and V. Mathew, "Investigation of CuAl IMCs Corrosion in Chloride Environment and Its Prevention Strategy." IMAPSource Proceedings (IMAPS Symposium): 000217–24. https://doi.org/10.4071/001c.74746, 2022.
[23] O.M. Chyan and M. Asokan, "United States patent application," US 2021/0071308, 2021.
[24] O. Cakir, "Copper etching with cupric chloride and regeneration of waste etchant," *Journal of Materials Processing Technology*, Vol. 175, pp. 63-68, 2006.
[25] UNT Center for Friction Stir Processing, Mini Tensile Testing System. https://cfsp.unt.edu/mini-tensile-testing-system-0.
[26] R.R. Tummala, E.J. Rymaszewski, and A.G. Klopfenstein, *Microelectronics Packaging Handbook, Part 2: Semiconductor Packaging*, Springer, Boston, MA, pp. 459, 1997.
[27] A. Kolics, A.S. Besing, P. Baradlai, R. Haasch, and A. Wieckowski, "Effect of pH on thickness and ion content of the oxide film on aluminum in NaCl media," *Journal of the Electrochemical Society*, Vol. 148, pp. B251, 2001.
[28] Z.Y. Hu, P.P. Wang, E.G. Fu, X.J. Wang, X.Q. Yan, P. Xu, Z.M. Wu, Y.B. Zhao, and Y.X. Liang, "Bilayer nanoporous copper films with various morphology features synthesized by one-step dealloying," *Journal of Alloys and Compounds*, Vol. 754, pp. 26-31, 2018.
[29] Y. Wu and A. Lee, "Corrosion-Induced mass loss of Cu9Al4 at the Cu-Al ball–bond interface: Explained based on full immersion of Cu, Al, and Cu-Al intermetallic galvanic couples," *Journal of Electronic Materials*, Vol. 48, pp. 44-52, 2019.
[30] P.M. Natishan and W.E. O'Grady, "Chloride ion interactions with oxide-covered aluminum leading to pitting corrosion: A review," *Journal of the Electrochemical Society*, Vol. 161, pp. C421-C432, 2014.
[31] A. El Warraky, H.A. El Shayeb, and E.M. Sherif, "Pitting corrosion of copper in chloride solutions," *Anti-Corrosion Methods and Materials*, Vol. 51, pp. 52-61, 2004.